The Deadliest Tornado (EF4) in the Past 40 Years in China

ZHIYONG MENG,[a] LANQIANG BAI,[a] MURONG ZHANG,[a] ZHIFANG WU,[b] ZHAOHUI LI,[c,d] MEIJUAN PU,[e] YONGGUANG ZHENG,[f] XIAOHUA WANG,[e] DAN YAO,[g] MING XUE,[h,i,j,k] KUN ZHAO,[h,i] ZHAOMING LI,[c] SIQI PENG,[b] AND LIYE LI[c]

[a] *Laboratory for Climate and Ocean–Atmosphere Studies, Department of Atmospheric and Oceanic Sciences, School of Physics, Peking University, Beijing, China*
[b] *Guangdong Meteorological Bureau, Guangdong, China*
[c] *Foshan Tornado Research Center, Guangdong, China*
[d] *Weathernews America Inc., Norman, Oklahoma*
[e] *Jiangsu Meteorological Bureau, Nanjing, China*
[f] *National Meteorological Center, Beijing, China*
[g] *State Key Laboratory of Severe Weather, Chinese Academy of Meteorological Sciences, Beijing, China*
[h] *Key Laboratory of Mesoscale Severe Weather, Ministry of Education of China, Nanjing University, Nanjing, China*
[i] *School of Atmospheric Sciences, Nanjing University, Nanjing, China*
[j] *Center for Analysis and Prediction of Storms, Oklahoma University, Norman, Oklahoma*
[k] *School of Meteorology, Oklahoma University, Norman, Oklahoma*

(Manuscript received 23 June 2017, in final form 11 March 2018)

ABSTRACT

An EF4 supercellular tornado hit Funing County, Yancheng, Jiangsu Province, China, from about 1410 to 1500 local standard time 23 June 2016, causing 98 fatalities and 846 injuries. It was the deadliest tornado in the past 40 years in China. This paper documents the storm environment, evolution of the radar signatures, real-time operational tornado warning services, and the damage distribution during this event. The tornado was spawned from a supercell that developed ahead of an upper-level trough extending southwestward from a low pressure vortex in northeast China and dissipated following the occlusion of the tornado vortex. The radar-based rotational velocity of the mesocyclone peaked at 42.2 m s^{-1}. The strength of the tornado vortex signature (gate-to-gate azimuthal radial velocity difference) peaked at 84.5 m s^{-1}. Surface observations at 1-min intervals from a mesoscale network of in situ surface weather stations revealed the surface wind pattern associated with the mesocyclone, such as convergent and rotational flows. The tornado formed after the peak updraft strength of the supercell, producing a damage swath that was 34.5 km long and with a maximum width of 4.1 km. The review of the tornado warning process for this event reveals that there is much work to be done to develop operational tornado forecast and warning services for China.

1. Introduction

On the afternoon of 23 June 2016, a violent tornado rated EF4 (Xue et al. 2016; Zheng et al. 2016) on the enhanced Fujita (EF) scale (WSEC 2006) occurred in Funing County of Yancheng City, Jiangsu Province, China (Fig. 1). The tornado caused 98 fatalities and 846 injuries in Funing County. Around 3200 residences, two primary schools, and eight factory warehouses were destroyed. It was the first tornado to hit Yancheng on that day. Another tornado was spawned by the same supercell in Sheyang County of Yancheng City ~10 min after the demise of the first tornado (Fig. 1). This paper mainly focuses on the first tornado, hereinafter referred to as the Funing tornado.

The 23 June 2016 Funing EF4 tornado was the deadliest tornado recorded in the past 40 years in China (Table 1). Although tornado occurrence frequency in China is relatively low compared with the United States, it is rather significant for East Asia (Markowski and Richardson 2010). According to the tornado statistics calculated by Fan and Yu (2015), the annual average frequency of tornadoes in China was at least 60 during 2004–13, which was less frequent than the 250 tornadoes per year reported in Europe during 2006–10 (Antonescu et al. 2017) and the at least 1000 tornadoes identified

Corresponding author: Dr. Zhiyong Meng, zymeng@pku.edu.cn

DOI: 10.1175/WAF-D-17-0085.1

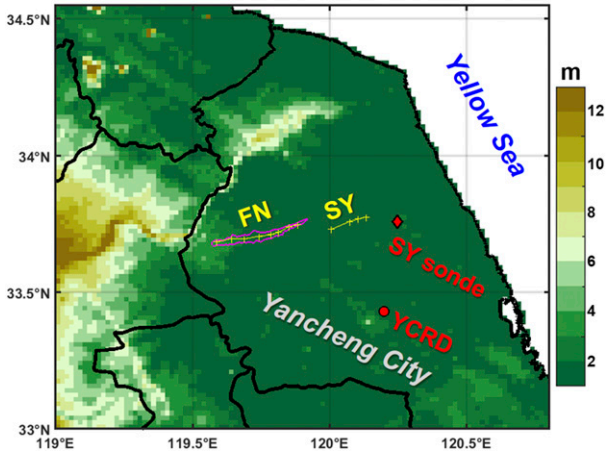

FIG. 1. Terrain height (shaded; m MSL) around Yancheng, Jiangsu Province. The yellow lines represent the path of 0.5° TVSs [yellow crosses; from the Yancheng radar (YCRD)] of the Funing (FN) tornado and the Sheyang (SY) tornado on 23 Jun 2016. The magenta contour represents the EF0 isopleth of the Funing tornado damage swath. The red diamond represents the location of the Sheyang radiosonde (SY sonde).

each year in the United States. The highest frequency of tornadoes in China occurs in July, with a secondary peak in April. Among all the provinces, Jiangsu Province has the highest frequency of tornadoes of various intensities (Fan and Yu 2015). As shown in Table 1, two of the top-10 deadliest tornadoes ever recorded in China occurred in Yancheng, Jiangsu Province. Besides tornadoes, Jiangsu Province also has the highest frequency of mesoscale convective systems (MCSs) in China (Meng et al. 2013; He et al. 2017), suggesting that the region is climatologically favorable for convective environments that support severe convective storms.

Because they are less frequent and cause less overall damage than heavy rainfall and flooding events, tornadoes have not received adequate attention in either the operational forecasting or research communities in China. In recent years, with the increased application of communication technology, especially the Internet and smartphones with digital cameras, the public and meteorologists have become more aware of tornadoes in China; in particular, the occurrence of several high-impact tornadoes in the past two years, including the 2 June 2015 Baicheng tornado in northeast China, the 4 October 2015 Foshan tornado in southeast China (Bai et al. 2017), the 5 June 2016 Wenchang tornado in southern China, and especially the 23 June 2016 Funing tornado in central-eastern China, have aroused concern from both the research community and the public.

To achieve the ultimate goal of an operational tornado forecasting and warning system, two important things must be achieved: 1) the development and maintenance of systematic documentation of tornado reports to establish a tornado database and 2) the construction of comprehensive case studies to better understand tornado features and their storm environments. Detailed analyses of the 21 July 2012 Beijing EF3 tornado and the 4 October 2015 Foshan, Guangdong, EF3 tropical cyclone–associated tornado were performed by Meng and Yao (2014) and Bai et al. (2017), respectively. However, to date, there is no detailed documentation of a violent (EF4+) tornado in China in the literature, especially in Jiangsu Province, where the climatological maximum for tornadoes in China occurs. This paper is aimed at documenting the storm environment (section 2), radar features (section 3), warning services issued by local meteorological agencies (section 4), and damage distribution (section 5) for the 23 June 2016 Funing EF4 tornado. A discussion and a brief summary are given in sections 6 and 7, respectively.

2. Synoptic and mesoscale environment

a. Synoptic environment

The Funing tornado occurred in a typical convection-producing synoptic environment. At 1400 local standard time (LST; LST = UTC + 8 h), ~10 min before the

TABLE 1. Top-10 deadliest tornadoes that have been recorded in China since 1951. The locations of the provinces in this table are given in Fig. 2b using their acronyms.

Date	Location	No. of fatalities	Intensity
22 Apr 1958	Hanchuan, Hubei (HB)	133	≥F3
16 Apr 1977	Huanggang, Hubei (HB)	103	≥F3
23 Jun 2016	Funing, Yancheng, Jiangsu (JS)	98	EF4
29 Aug 1969	Baxian, Tianjin (TJ)	>94	≥F3
14 Apr 1978	Xianyang, Shanxi (SX)	84	
31 Jul 1964	Xiaogan, Hubei (HB)	82	
27 Apr 1983	Xiangyin, Hunan (HN)	81	
3 Mar 1966	Yancheng, Jiangsu (JS)	74	≥F4
5 Jul 1958	Zaozhuang, Shandong (SD)	63	
17 Apr 1979	Changde, Hunan (HN)	59	

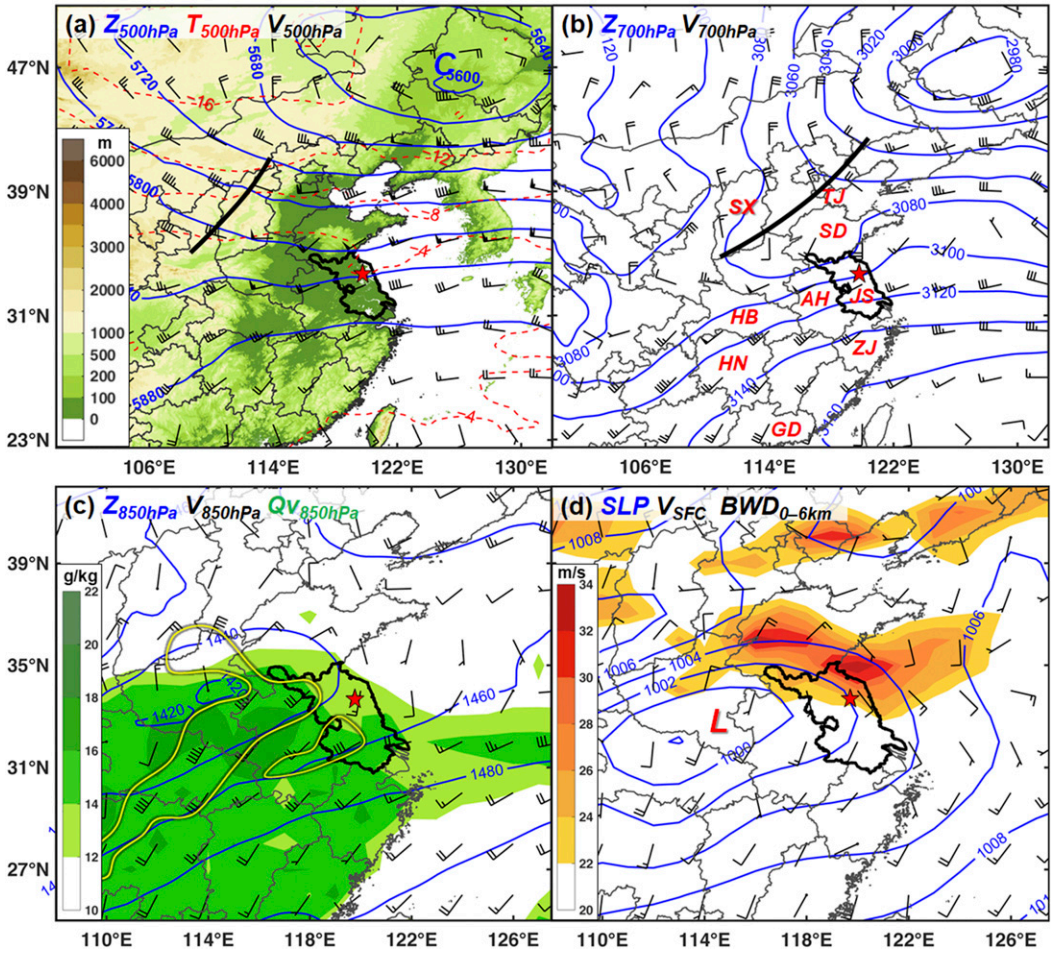

FIG. 2. NCEP FNL analysis valid at 1400 LST 23 Jun 2016. (a) Geopotential heights (blue; gpm), temperature (red; °C), and winds at 500 hPa. The thick black line denotes the 500-hPa trough. Terrain height (m MSL) is shaded for reference. The 500-hPa cold vortex center is labeled by C in blue. (b) Geopotential heights (blue; gpm) and winds at 700 hPa. The thick black line denotes the 700-hPa trough. The locations of Tianjin (TJ), Shandong (SD), Shanxi (SX), Anhui (AH), Jiangsu (JS), Hubei (HB), Hunan (HN), Zhejiang (ZJ), and Guangdong (GD) Provinces are labeled. (c) Geopotential heights (blue; gpm), specific humidity (shaded; g kg^{-1}), and winds at 850 hPa. The 850-hPa jets (>12 m s^{-1}) are contoured in yellow. (d) Sea level pressure (blue; hPa), surface winds, and 0–6 km AGL bulk wind difference (BWD; m s^{-1}) with magnitudes greater than 22 m s^{-1} shaded. The surface low center is labeled by L. In all panels, half barbs, full barbs, and pennants denote 2, 4, and 20 m s^{-1}, respectively. The location of the Funing tornado is denoted by a red star. Jiangsu Province is outlined in bold.

tornadogenesis, Yancheng was located in front of a shallow 500-hPa trough extending from a quasi-stationary cold vortex in northeast China (Fig. 2a). A cold vortex is characterized by a synoptic cyclonic vortex with a local cold core in the middle and upper troposphere (Xie and Bueh 2015). It is usually responsible for series of severe convective weather events in northern China during the summer. At lower levels, Yancheng was characterized by a distinct 700-hPa trough to the northwest (Fig. 2b) and 850-hPa jets to the southwest that provided strong moisture convergence over the city (Fig. 2c). Below these low-level jets, a distinct northeast–southwest-oriented surface low was observed in central China (Fig. 2d). Yancheng was located at the inverted trough of the low pressure zone. In such a large-scale environment, the 0–6-km bulk wind difference near Yancheng increased from less than 10 m s^{-1} at 0800 LST 23 June 2016 (not shown) to greater than 23 m s^{-1} at 1400 LST 23 June 2016 (Fig. 2d).

b. *Mesoscale atmospheric environment*

The Funing tornado was spawned by a supercell that developed at the southern end of a northwest–southeast-oriented linear MCS (denoted by B in Fig. 3a), which developed in front of a much longer quasi-linear MCS (denoted by A in Fig. 3a). MCS A was accompanied by a cold front and had a trailing stratiform precipitation

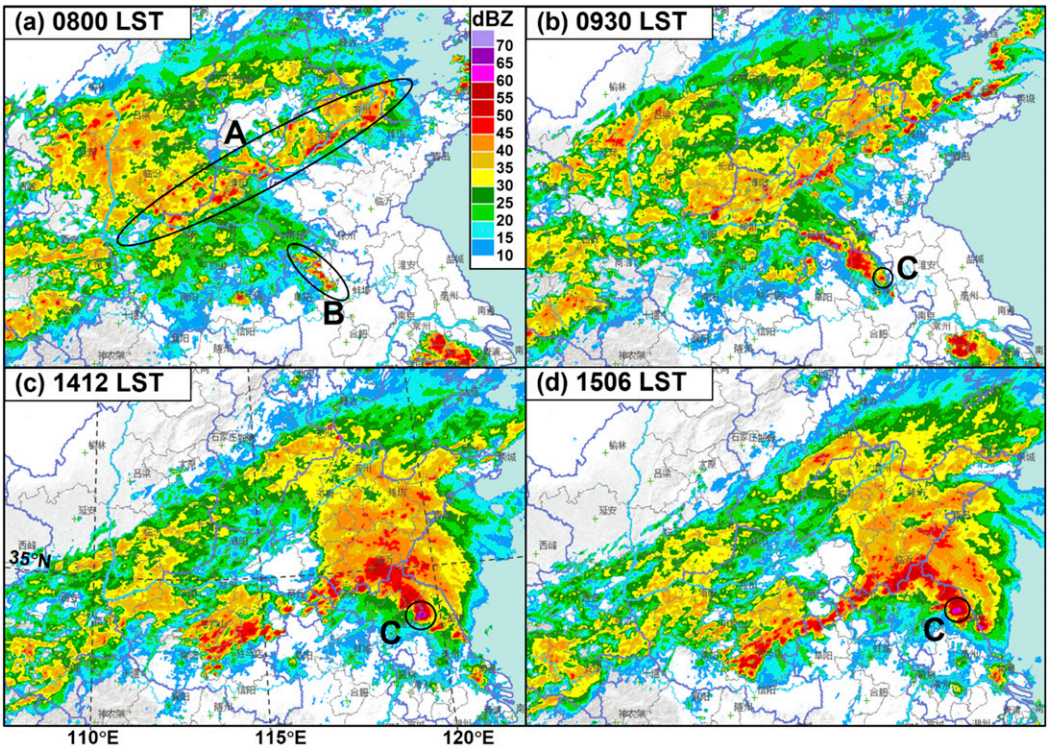

FIG. 3. Mosaic of composite radar reflectivity (dBZ) at (a) 0800, (b) 0930, (c) 1412, and (d) 1506 LST 23 Jun 2016. Capital letters A and B denote the southwest–northeast- and northwest–southeast-oriented convective lines, respectively. The small black circle and capital letter C in (b)–(d) denote the tornadic supercell.

region, while MCS B formed in the warm sector and had a leading stratiform precipitation region from ~1100 LST (e.g., Fig. 3). The tornadic supercell storm (denoted by C in Fig. 3b) initiated in northern Anhui Province at about 0912 LST. It then moved to the northeast with MCS B, intensified, and produced the Funing tornado from ~1410 to 1500 LST (Figs. 3c,d).

A mesoscale network (mesonet) of in situ surface weather stations was available from Jiangsu Meteorological Bureau for the duration of this event. These stations are deployed with a horizontal spacing of about 4–30 km in Jiangsu Province and report some basic meteorological factors including temperature, dewpoint, and 10-m winds at 1-min intervals. Relative humidity is also collected by a few stations. Unfortunately, pressure is not collected; therefore, the pressure-related thermodynamical variables were not available for this study. The mesoscale environmental features around the storm were examined using the available surface observations.

About 1 h before the Funing tornado formed, the region around the Funing and Sheyang tornadoes was characterized by a northwest-oriented surface warm tongue (Fig. 4a). Under the circumstances, the storm was moving into a positive surface temperature gradient zone (with respect to the storm translation direction), which could result in larger CAPE to support the maintenance and enhancement of the storm's main updraft (or mesocyclone). From 1351 LST, a well-defined hook-echo signature developed rapidly (not shown).

The juxtaposition between the surface temperature field and the two tornado paths was consistent with the Funing tornado being stronger than the Sheyang tornado. Before the Funing tornadogenesis, the supercell moved into a more unstable zone (Fig. 4). However, the supercell moved toward a less unstable zone before the Sheyang tornadogenesis. Located in a less-unstable environment, the updrafts of the supercell during the Sheyang tornado stage were weaker as compared with those during the Funing tornado stage, which will be discussed in the next section.

A balloon radiosonde that was launched at 1400 LST 23 June 2016 in Sheyang (red diamond in Fig. 4), about 63 km to the northeast of the Funing tornadogenesis location, was available. To depict the near-storm environment, the sounding was modified with the mean surface temperature T_{sfc} and dewpoint T_d of several stations located in the inflow region and close to the hook-echo signature (these stations are denoted by red dots in Fig. 4b). Assuming a well-mixed planetary

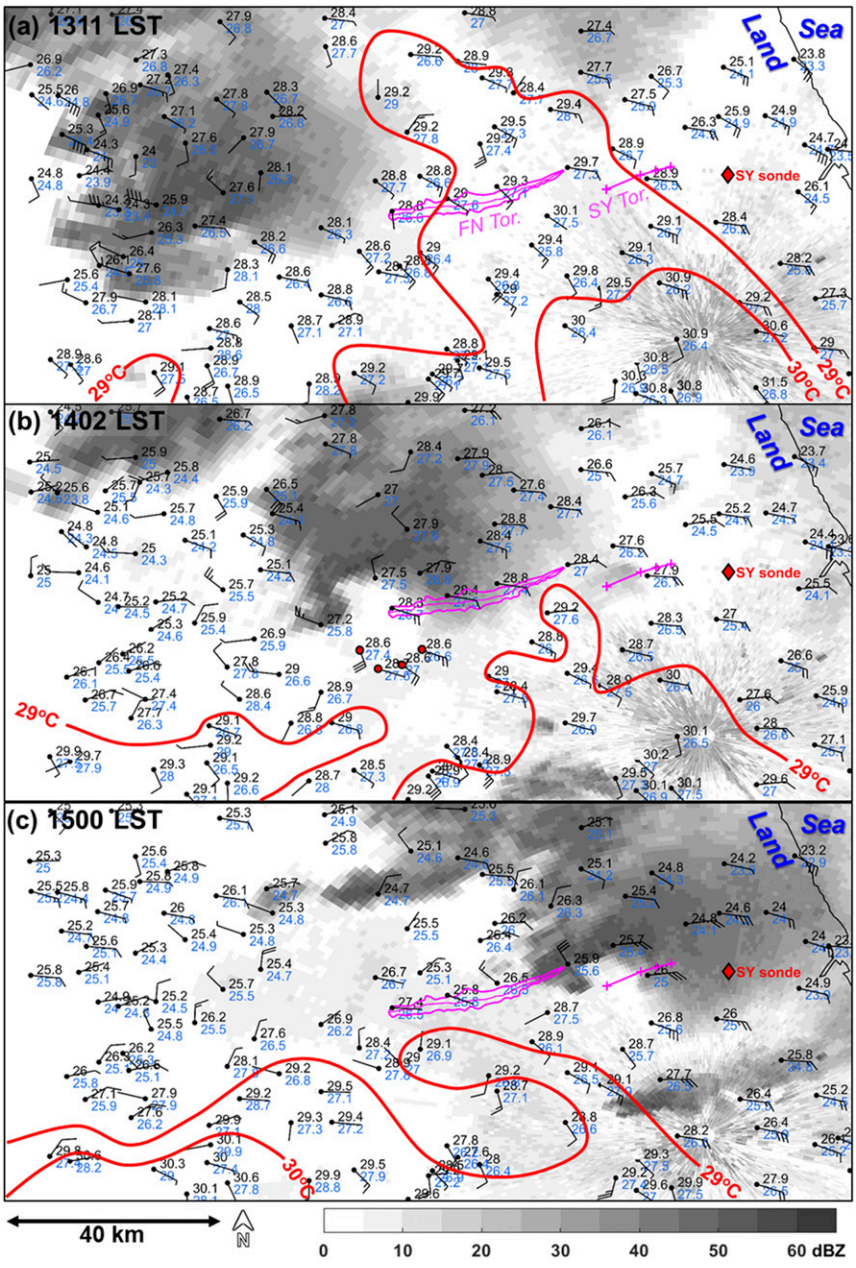

FIG. 4. Observations [wind gust, temperature (black text; °C), and dewpoint (blue text; °C)] from in situ surface weather stations. Also shown are base reflectivity (shading; dBZ) at the 0.5° elevation angle from the Yancheng radar. Half barbs, full barbs, and pennants denote 1, 2, and 10 m s^{-1}, respectively. Surface temperatures of 29° and 30°C are contoured in red. The locations of the Funing tornado (FN Tor.) and Sheyang tornado (SY Tor.) are denoted in magenta. The red diamond represents the location of the Sheyang radiosonde (SY sonde). Red dots in (b) denote the surface weather stations described in the caption of Fig. 5. The north direction and distance length scale are given at the bottom.

boundary layer with a potential temperature equal to the average surface value (T_{sfc} = 28.6°C, T_d = 27.1°C), the surface-based CAPE reached 3290 J kg^{-1} with a small CIN of 5 J kg^{-1} [the upper-level gaps of the sounding were filled with the values from the NCEP Final (FNL) operational global analysis dataset (gridded onto a 1° × 1° grid) valid at 1400 LST at the Sheyang radiosonde location] (Fig. 5). The sounding showed a 0–6 km AGL layer bulk wind difference of 27.2 m s^{-1} and a strong directional shear in the lowest 1 km of the

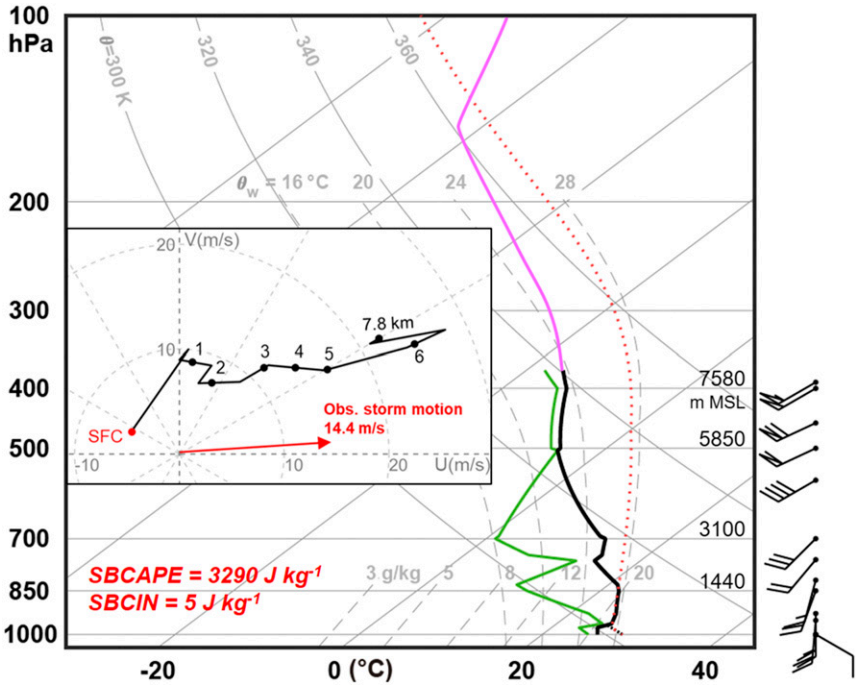

FIG. 5. Skew T–log$p$ and hodograph (inset) diagrams of the Sheyang radiosonde (the red diamond in Fig. 4) at 1400 LST 23 Jun 2016. The ambient temperature and dewpoint are represented by the solid black and green lines, respectively. To obtain a more representative storm environment, the sounding was modified by assuming a well-mixed boundary layer using the mean surface values at four stations (red dots in Fig. 4b). The modified ambient temperature is plotted as a dotted black line, and the parcel that ascends undiluted from the surface is shown by the dotted red line. The upper-level ambient temperature, which was missing in the radiosonde observation, was filled with values obtained from the NCEP FNL analysis at the Sheyang sounding location at 1400 LST 23 Jun 2016 (magenta). Half barbs, full barbs, and pennants denote 2, 4, and 20 m s^{-1}, respectively. The observed storm motion was obtained by tracking the centroid of the radial velocity maxima couplet of a 2.4° mesocyclone signature (at about 3 km AGL) from 1405:02 to 1433:30 LST.

atmosphere (Fig. 5). The 0–1-km storm-relative helicity (SRH) reached 139 m^2 s^{-2}, which is between the 50th and 75th percentiles (89.2–178 m^2 s^{-2}) of a significantly tornadic supercellular environment in the United States (Fig. 6a; Rasmussen 2003). The 0–3-km SRH reached 170 m^2 s^{-2}, which falls close to the median (180 m^2 s^{-2}) of the U.S. climatology (Rasmussen and Blanchard 1998). The lifting condensation level (LCL) was much lower than that in U.S. significant supercellular tornado cases as indicated by Rasmussen and Blanchard (1998) (Fig. 6a). Under these environmental conditions, at least three supercells developed that day, of which only the supercell discussed in this paper was tornadic.

3. Radar analysis

During this event, the radar closest to the Funing tornado was the Yancheng radar (Fig. 1), which was located about 51 km to the southeast of the midpoint of the tornado damage path. This radar is similar to the Weather Surveillance Radar-1988 Doppler (WSR-88D) used in the United States, in terms of both hardware and software (Zhu and Zhu 2004), and was operating in volume coverage pattern 21 (VCP21) during this event, scanning nine elevation angles of 0.5°, 1.4°, 2.4°, 3.3°, 4.3°, 6°, 9.9°, 14.6°, and 19.5° with a volumetric update time of approximately 6 min. The elevation of the radar antenna is 28.3 m above mean sea level (MSL). The radar data are sampled every 1° in the azimuth. The range from the radar to the Funing tornado varied from ~63 km (near the location of tornadogenesis) to ~45 km (near the location of tornado demise). The Nyquist velocity is 27.82 m s^{-1}. The range resolution is 1 km (250 m) for reflectivity (radial velocity). There was no azimuthal oversampling of the radar, and the azimuthal gate spacing at a range of 45 (60) km was ~785 (1050) m. The 0.5° radar beam was around 600 m over the surface at the location of the damage area.

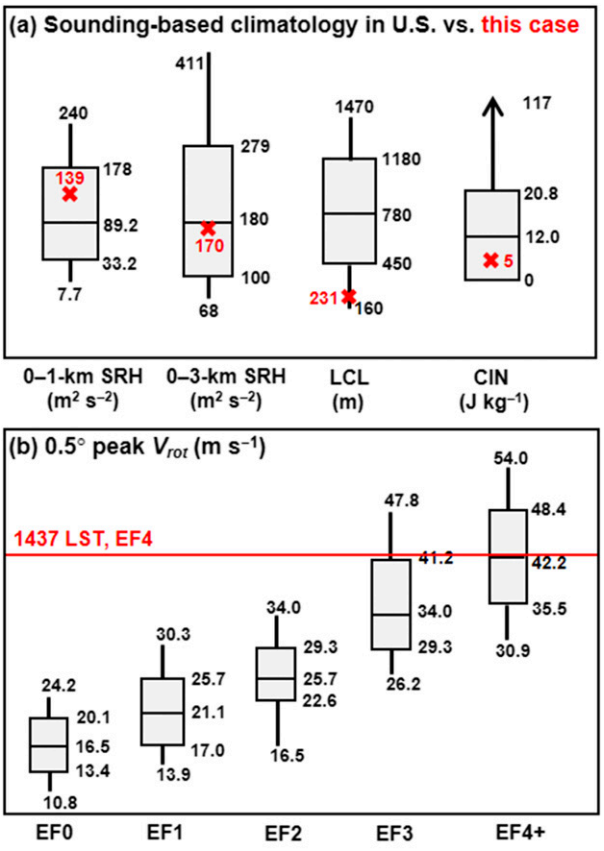

FIG. 6. (a) Comparison of the parameters of the Funing tornadic environment (red X) calculated with the radiosonde observation in Fig. 5 with the U.S. climatology for a supercellular tornado environment given by Rasmussen and Blanchard (1998) (box-and-whisker plot; adapted from their Figs. 4, 15, and 16) and Rasmussen (2003) (adapted from their Fig. 1). Parameters include 0–1 km AGL SRH ($m^2 s^{-2}$), 0–3 km AGL SRH ($m^2 s^{-2}$), LCL (m), and CIN ($J kg^{-1}$). (b) Box-and-whisker plot for 0.5° peak rotational velocity V_{rot} ($m s^{-1}$) of EF0–EF4+ tornado events reported in the contiguous United States during 2009–13 at 100–2900 ft ARL, which were adapted from Smith et al. (2015). The 0.5° peak V_{rot} of the Funing tornado event at 1437 LST (red line) is plotted onto the box-and-whisker plot for comparison. In the box-and-whisker diagrams, the percentile extents and corresponding values represent the 25th–75th percentiles for boxes, the 10th–90th percentiles for whiskers, and the 50th percentiles for lines in boxes.

The mesocyclone of the supercell was first identified at ~1340 LST when the rotational velocity V_{rot} [determined by the two-dimensional maximum V_{max} and minimum V_{min} radial velocity couplet (with a diameter of 2–10 km); $V_{rot} = |V_{max} - V_{min}|/2$] started to meet the mesocyclone threshold of $15 m s^{-1}$ (as defined by Richter et al. 2017) and have a vertical extent greater than 3 km (from 1.1 to 5.4 km AGL) (diamonds in Fig. 7). The radar-derived rotational velocity of the mesocyclone in this study was identified manually. About 30 min before the first detection of the mesocyclone by the Yancheng radar, the per minute surface wind observations captured the cyclonic rotational and convergent flow in an area with a diameter of about 25 km at 1311 LST (Fig. 8a). The mesocyclone signature started to appear at the 0.5° elevation angle at 1340 LST (Fig. 7). At this time, a 0.5° tornado vortex signature (TVS) was also detected. The gate-to-gate azimuthal radial velocity difference (DV) of a manually identified TVS in this study was required to be no less than $20 m s^{-1}$ (e.g., French et al. 2013; Meng and Yao 2014; Bai et al. 2017). After ~1354 LST, the mesocyclone intensified and extended upward, while its evolution at low levels was not clear because of obscuration by range-folded data.

The mesocyclone signature evidently intensified, especially above 5 km AGL, from ~1400 LST (Fig. 7). The rotational and convergent winds associated with the mesocyclone were captured well by the 1-min surface observations. A wind gust of $15 m s^{-1}$ with a sharp decrease in surface temperature and dewpoint was observed at station M6309 (Fig. 9a). Six minutes later, at 1406 LST, the mesocyclone reached its highest measurable altitude of approximately 8 km AGL (Fig. 7). Unfortunately, it was not possible to detect the TVS during the two volume scans at 1402 and 1408 LST because of obscuration by the range-folded data. A quite strong 0.5° TVS ($DV = 59 m s^{-1}$) was identified at ~1414 LST when apparent damage started to be observed on the ground. Almost simultaneously, station M5325 recorded an apparent enhancement of wind gusts (Fig. 9b).

The TVS reached its peak intensity at 1437 LST, with a gate-to-gate azimuthal radial velocity difference of $84.5 m s^{-1}$ (Fig. 7). The 0.5° peak rotational velocity (peak $V_{rot} = |V_{max} - V_{min}|/2$; only for velocity maxima with cyclonic azimuthal shear within 10 km) also reached its maxima of $42.25 m s^{-1}$ (the same radial velocity pixels as TVS) at this time, which is close to the median of 0.5° peak V_{rot} associated with EF4+ tornadoes in the U.S. climatology (Smith et al. 2015; their Fig. 5) (Fig. 6b). The TVS extended from the surface all the way up to about 12 km AGL.

The diameter of the mesocyclone, which is determined by the horizontal distance between the centers of the couplet of maximum and minimum radial velocities, was observed to diminish from 1406 to 1434 LST, as shown by the black circles in Figs. 10a–c. The hook echo also became increasingly curved (Figs. 8b–d). The mesocyclone reached its maximum rotational velocity of $42.2 m s^{-1}$ at the 0.5° elevation angle at 1426 LST (Fig. 7). After 1431 LST, the diameter of the mesocyclone contracted to less than 2 km at the 0.5° elevation angle and thus could not be considered as a mesocyclone, although the rotation was still strong. During

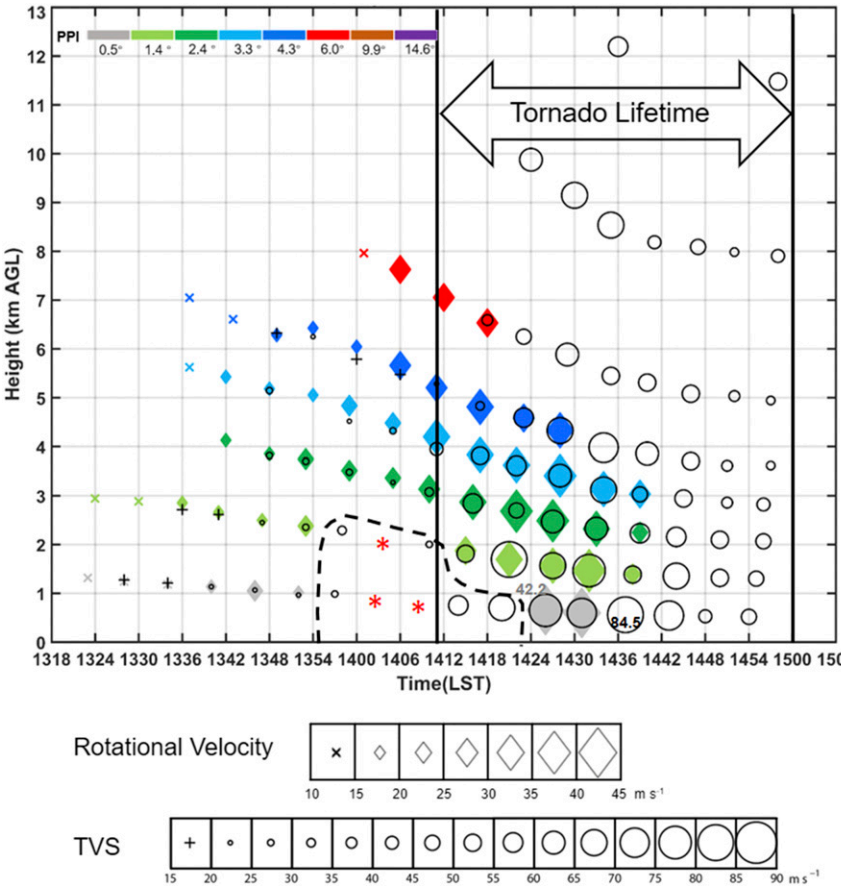

FIG. 7. Time–height evolution of the maximum gate-to-gate radial velocity difference of the TVS (circles; m s^{-1}) and the rotational velocity of the mesocyclone (diamonds with different colors denoting different elevation angles; m s^{-1}) manually identified from the Yancheng radar on 23 Jun 2016. The mesocyclone in the area circled by the dashed line could not be accurately identified because of obscuration by range-folded data. Similarly, red asterisks represent that the TVS could not be identified because of obscuration by range-folded data.

1434–1440 LST, new mesocyclone signatures were identified at different radar elevation angles (blue circles in Figs. 10c,d) closer to the parent supercell as the original tornado vortex moved rearward and became surrounded by downdrafts (e.g., Figs. 10g,h). The new mesocyclone then moved to the east (Figs. 10e,f), became more collocated with the hook echo, and later produced the Sheyang tornado.

The storm updraft strength was characterized by two peaks during the Funing tornado time period. In this study, the updraft strength was evaluated by radar updraft proxies: the maximum estimated size of hail (MESH) and the height of the 50-dBZ echo isosurface around the mesocyclone or the weak-echo region (WER) signatures (WDTD 2017). These updraft proxies were obtained from Gibson-Ridge Analyst, version 2 (GR2Analyst 2.0; http://www.grlevelx.com/gr2analyst_2/). From when the mesocyclone signature was identified (~1340 LST), the maximum height of the 50-dBZ echo isosurface and the maximum MESH both increased abruptly, suggesting a rapid enhancement of the main updraft of the supercell (Fig. 11). Near the time of the Funing tornadogenesis (~1410 LST), the updraft strength reached its first peak, with a 50-dBZ echo top of 17.2 km above radar level (ARL) and a maximum MESH of 12.7 cm. The storm updraft strength evidently decreased after the Funing tornadogenesis until 1437 LST, when the storm updraft intensified again and peaked at ~1450 LST, probably associated with the development of the new mesocyclone in the same supercell. The storm updraft during the Sheyang tornado period (~1510–1530 LST) was not as strong as that in the Funing tornado period, which was likely because the supercell moved into a less unstable zone (Fig. 4).

The trend in the storm updraft strength agreed well with the narrowing and expansion of the size of the

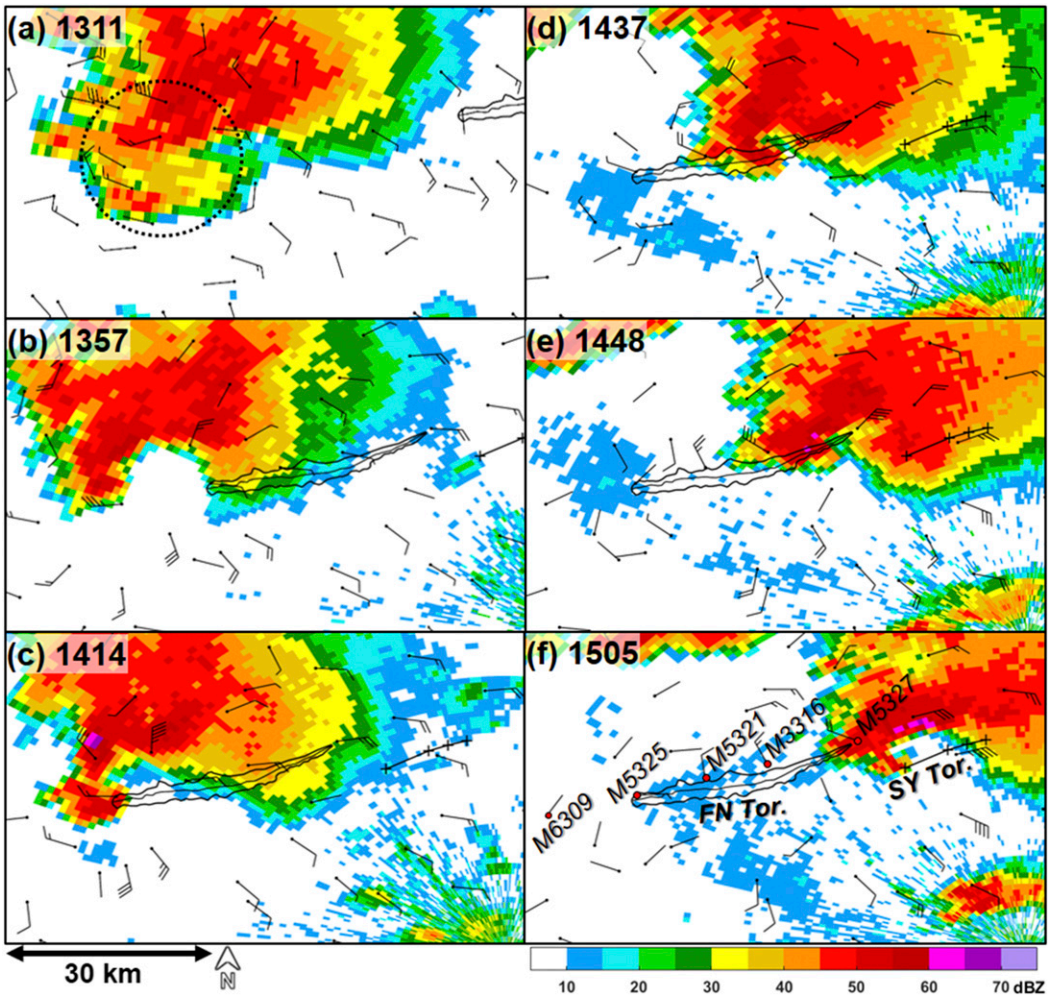

FIG. 8. Base reflectivity (shaded; dBZ) at the 0.5° elevation angle from the Yancheng radar at different times (LST) on 23 Jun 2016. Also plotted are surface gusts (half barb, 1 m s^{-1}; full barb, 2 m s^{-1}; pennant, 10 m s^{-1}) at the same time. The EF0 isopleth of the Funing tornado damage swath and the analyzed tornado track are both given by a black curve. The path of 0.5° TVSs (black crosses) of the Sheyang tornado (SY Tor.) are also denoted. The dotted circle in (a) denotes the area where there are convergent and rotational wind patterns, as described in the text. The locations of surface weather stations (red dots) described in Fig. 9 are given in (f). The north direction and distance length scale are given at the bottom.

WER signature during the Funing tornado time period. A well-defined WER signature was observed starting at 1351 LST. The horizontal and vertical spatial extent of this WER signature decreased after the genesis of the Funing tornado and reached a minimum at 1437 LST, which was approximately the midpoint of the tornado's life-span (Figs. 8b–f and Fig. 12). The WER signature was bounded above 4 km ARL (using 40-dBZ contours) at 1414 LST, whereas at 1437 LST, the height of the bounded WER dropped to below 3 km (Figs. 12a,b). After 1437 LST, the horizontal and vertical spatial extents of this WER signature began to expand again (Figs. 8d–f and Figs.12b–d), which suggests updraft restrengthening. This restrengthening was likely associated with the occlusion process leading to the second tornado near Sheyang.

The contraction of the width of the mesocyclone and its subsequent evolution at low levels further implied that there was an occlusion process in the tornado vortex, which was responsible for the weakening of the Funing tornado. The TVS associated with the Funing tornado moved rearward into the rear-flank downdraft region during the tornado weakening stage (e.g., Figs. 10g,h). After 1457 LST, the TVS lost its identity at all elevation angles and stopped producing EF0+ damage at the surface. An apparently smaller surface gust was observed at station M5327 (relative to other stations) (Fig. 9c), which was located about 1 km east of

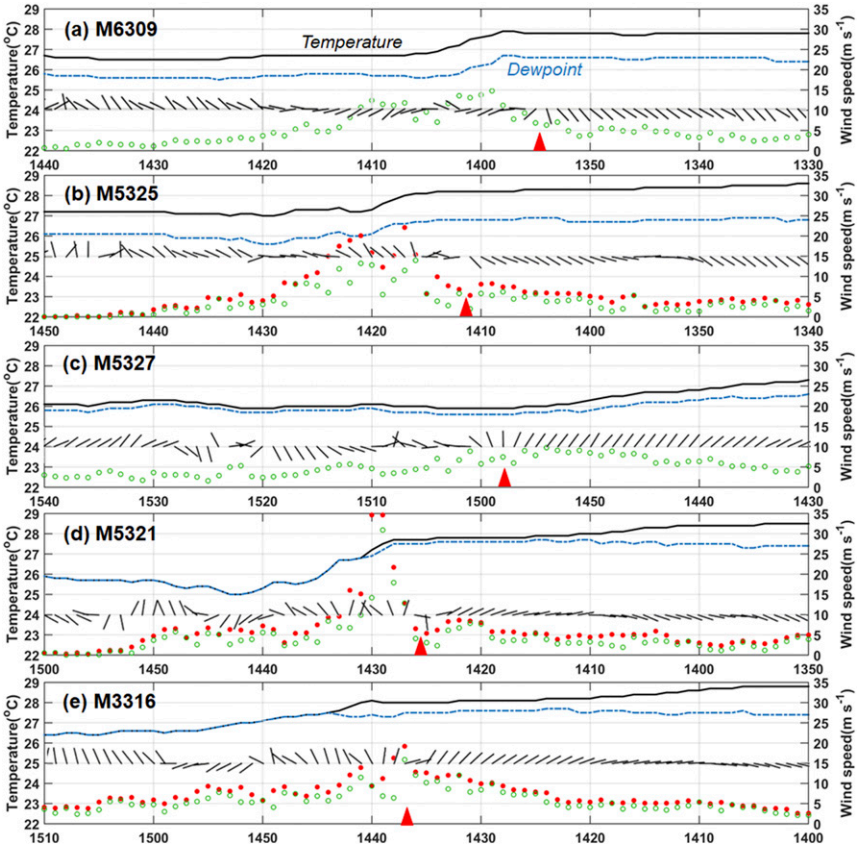

FIG. 9. Meteogram of surface temperature (black curves; °C), dewpoint (blue curves; °C), gust direction (black bars along a straight line, pointing to the wind direction from the line), and speed (green circles), as well as the maximum gust speed in the past 1 min (red dots) at several stations (shown in Fig. 8f). The time increases from right to left. The red triangle denotes the time when an apparent wind shift occurred.

the endpoint of the damage swath (Fig. 8f), although there was still an apparent rotational wind shift during 1455–1505 LST. Consequently, the demise of the Funing tornado was probably a result of a mismatch between the horizontal motions of the tornado vortex and the main storm-scale updraft of the parent supercell. Such a horizontal motion mismatch was likely because of the occlusion process in the tornado vortex due to the rear-flank gust front that wrapped cyclonically ahead of the tornado (e.g., Dowell and Bluestein 2002a,b).

4. Warning services

In a province in China, there are three levels of meteorological observatories, namely, province, city, and county levels. A province-level observatory issues a warning when at least three cities in the province will be affected by severe weather. A city-level observatory issues a warning when at least two counties of the city will be affected by severe weather. A county-level observatory issues a warning for the county itself. A lower-level observatory usually issues warnings in more detail and has a more direct contact channel with the people in the warning area than do the higher-level observatories.

A platform named Severe Weather Alert and Track Comprehensive (SWATCH) provides warning decision-making guidance for the forecasters in Jiangsu Province, in addition to conventional raw observations. SWATCH is a platform that efficiently displays the most important storm information. It was developed by the Jiangsu Meteorological Bureau and put into practice in April 2015. SWATCH rapidly integrates storm radar products from 12 Doppler radars deployed in Jiangsu Province and the neighboring areas. The radar products are produced by a special radar processor (with data quality control) named the ''principal user processor'' (PUP), which was designed for analyzing raw data from the China New Generation Weather Radar (CINRAD). By combining the storm products of multiple radars from

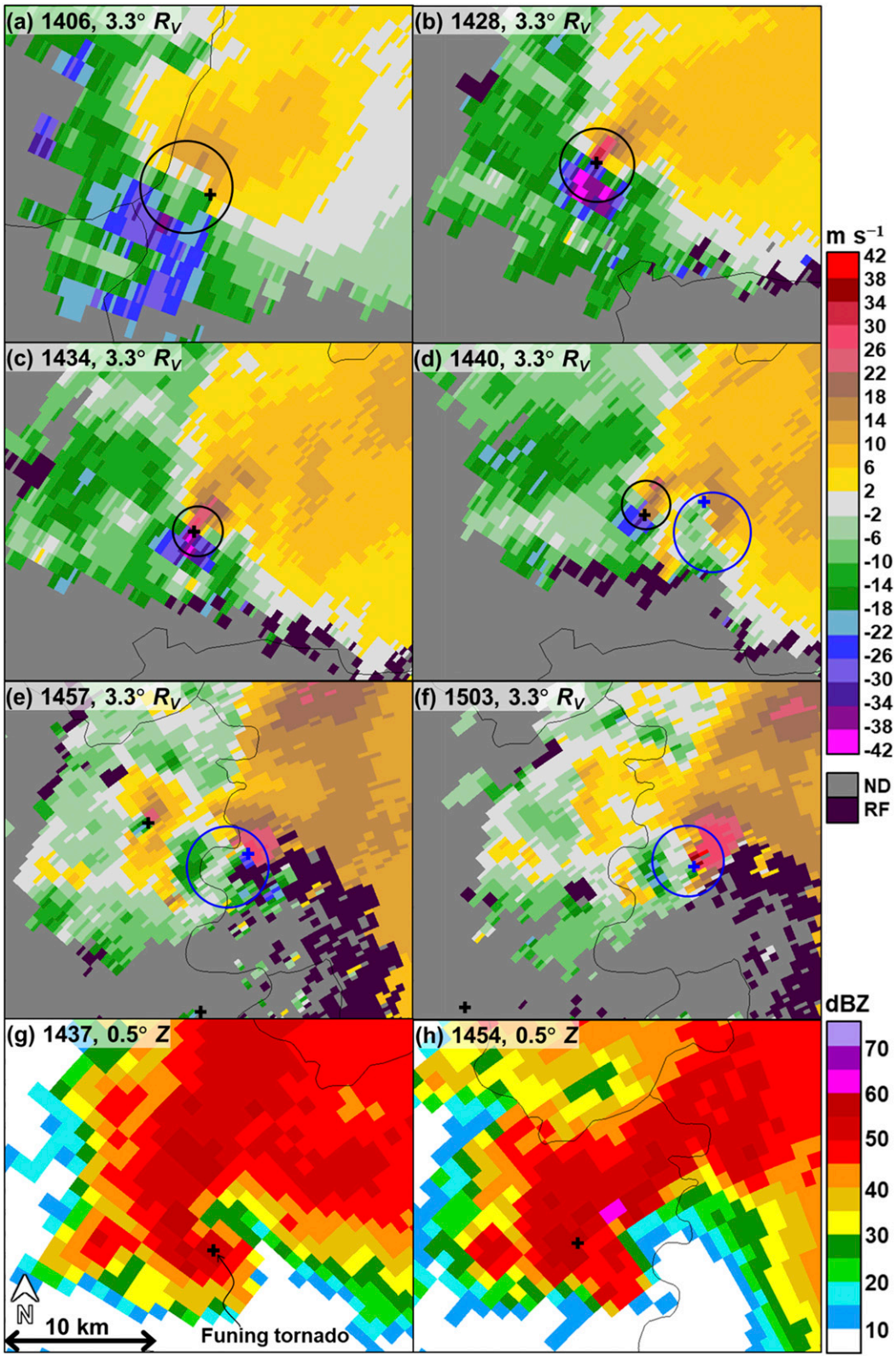

FIG. 10. (a)–(f) Radial velocity R_v (m s^{-1}) at the 3.3° elevation angle and (g),(h) base reflectivity Z (dBZ) at the 0.5° elevation angle from the Yancheng radar at different times (LST) on 23 Jun 2016. The locations of the TVS and mesocyclone associated with the Funing (Sheyang) tornado at the given elevation angle are marked by a black (blue) cross and circle, respectively. The 3.3° radial velocity fields are given because they were not apparently affected by obscuration by range-folded data. For all panels, the north direction and distance length scale are given at the bottom in (g).

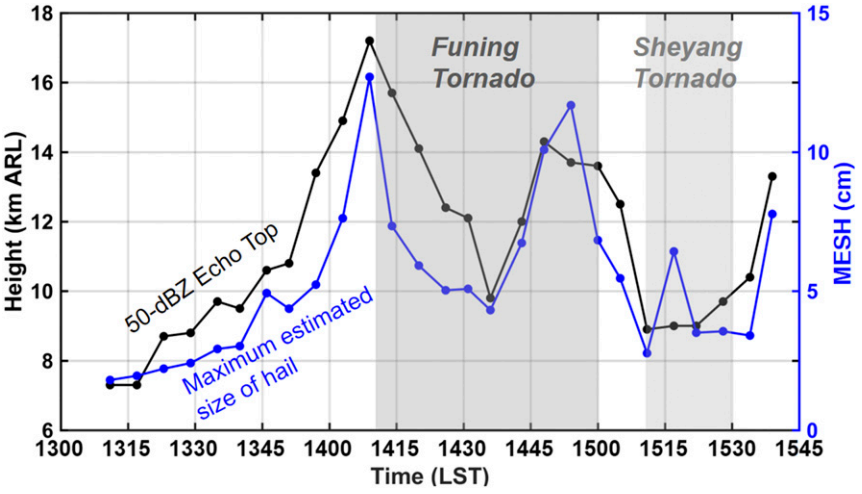

FIG. 11. Meteogram of the maximum height of the 50-dBZ echo isosurface (black; km ARL) and the MESH (blue; cm) around the mesocyclone or WER signatures of the supercell that produced the Funing and Sheyang tornadoes. The life-spans of the Funing and Sheyang tornadoes are shaded in gray.

PUP, SWATCH can save forecasters' time in switching from one radar to another. SWATCH infers a tornado based on the base height and wind shear criteria of the mesocyclone signature, as well as storm structure products from PUP: 1) the mesocyclone signature is sustained for at least two consecutive volume scans, 2) the base height of the mesocyclone signature is <1.2 km ARL, and 3) the wind shear is $>22 \times 10^{-3}\,s^{-1}$. The mesocyclone signature displayed on PUP is taken from the mesocyclone detection algorithm (MDA) developed by NSSL (Stumpf et al. 1998). In addition to detecting a potential tornado, SWATCH also displays extreme values of surface observations, such as rain rate, wind gusts (force 6 and above on the Beaufort scale within the past 30 min), hail, and lightning. As SWATCH only shows the extreme values of observations, it cannot capture the convergent and rotational wind patterns in a timely manner. SWATCH combines algorithm information to provide detailed storm information displays using graphs and tables, and it can automatically generate textual alerts. This information is used as warning decision-making guidance for the forecasters.

The real-time nowcast and warning services in this event were quite successful for the severe weather hazards but understated the tornado risk. The Jiangsu Province–level meteorological observatory made a nowcast at 1230 LST that gusts of up to force 6 on the Beaufort scale, lightning, and 20–50 mm of rainfall might occur in 26 cities and counties in northern Jiangsu Province within the next 2 h. At 1257 LST, which was about 1 h prior to the Funing tornadogenesis, the Funing County–level meteorological observatory issued a thunderstorm warning stating that lightning, gusts of force 9 and above on the Beaufort scale, and rainfall of $>20\,mm\,h^{-1}$ might occur in most areas of the county within 6 h.

At 1400 LST, a forecaster on duty at the Jiangsu Province–level meteorological observatory noticed a convergent wind pattern reflected by two surface gust observations of 16.6 and $16.8\,m\,s^{-1}$ at ~1350 LST around the hook echo of the supercell (not shown). The forecaster then realized that the low-level main updraft of the supercell probably had been enhanced but was not confident enough to mention the potential of a tornado in the thunderstorm warning until 1426 LST, when SWATCH inferred a tornado about 16 min after the actual tornadogenesis. At this time, the mesocyclone was at its peak intensity, with a base down to 0.7 km AGL and a wind shear of $79 \times 10^{-3}\,s^{-1}$. In the meantime, a gust of $34.6\,m\,s^{-1}$ was observed at station M5321 (Fig. 9d) about 2 km north of the tornado centerline (Fig. 8f). According to the potential tornado detected by SWATCH, the Jiangsu Province–level meteorological observatory made a nowcast at 1430 LST that nine counties, including Funing and Sheyang, might be affected by 50–70 mm of rainfall, lightning, 2–5-mm hail, gusts of force 9 and above on the Beaufort scale, and an F2 tornado on the Fujita scale within 2 h. A similar nowcast with stronger gusts of force 10 and above on the Beaufort scale was then made by the Yancheng City–level meteorological observatory at 1435 LST for 16 towns in Funing County. Finally, at 1439 LST, the Funing County–level meteorological observatory updated their previous thunderstorm warning to mention the possibility of a developing tornado. This warning was issued already ~30 min after the Funing tornadogenesis

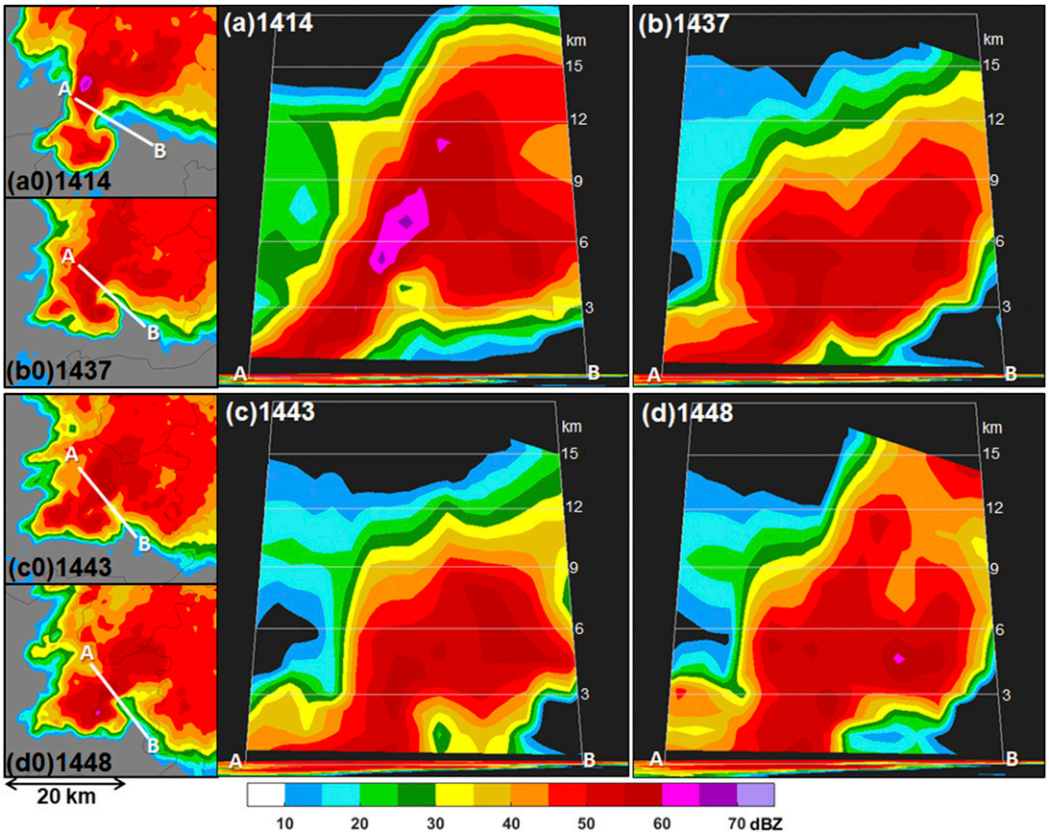

FIG. 12. (a)–(d) Vertical cross sections of radar reflectivity along the A–B lines as shown in the (a0)–(d0) 0.5° radar reflectivity, respectively, at different times (LST) on 23 Jun 2016.

but still 20 min before the demise of the Funing tornado and ~30 min before the Sheyang tornadogenesis.

It is important to note that, unlike in the United States and some other countries, there are no specific tornado warning products issued in the severe weather alert system in China, which is likely because of the rare occurrence of tornadoes relative to those countries. Instead, the potential for a tornado may be mentioned in a thunderstorm warning together with the potential for wind gusts, torrential rain, hail, and lightning.

5. Damage survey

Damage features of the Funing tornado were analyzed using information collected through four day-long ground and aerial damage surveys from 24 to 27 June 2016. Damage surveys were conducted only for the high-impact Funing tornado because the damage caused by the Sheyang tornado had already been cleared up by the time the Funing tornado surveys were completed. The damage surveys were performed under the collaboration of Peking University, the Foshan Tornado Research Center, China Meteorological Administration (CMA), the Jiangsu Meteorological Bureau, and Nanjing University. In the ground survey, the locations of damage indicators (DIs) and the direction of fallen trees and transmission towers (or poles) were determined by handheld GPS devices and compasses, respectively. At least three photos were taken to record each ground-surveyed fallen tree (or transmission structure) and its location and fallen direction. The location errors of these recorded DIs in Google Earth were generally within 10 m (mostly less than 5 m) and were determined by checking the locations of some isolated landmarks (e.g., trees and transmission towers) recorded by GPS devices. All of the information was then checked using the videos (if the same DI was captured) obtained from the aerial survey to avoid incorrect manual records during the ground survey, such as the DI location or tree-fall direction. The aerial survey was performed with a quadcopter drone (DJI Inspire 1 Pro) equipped with a camera that has 4K video recording capability. The drone flew steadily at about 100–400 m AGL to obtain damage information with different levels of detail. The recorded 4K videos, with a total time length of 5.13 h, covered almost the entire damage area of the Funing tornado.

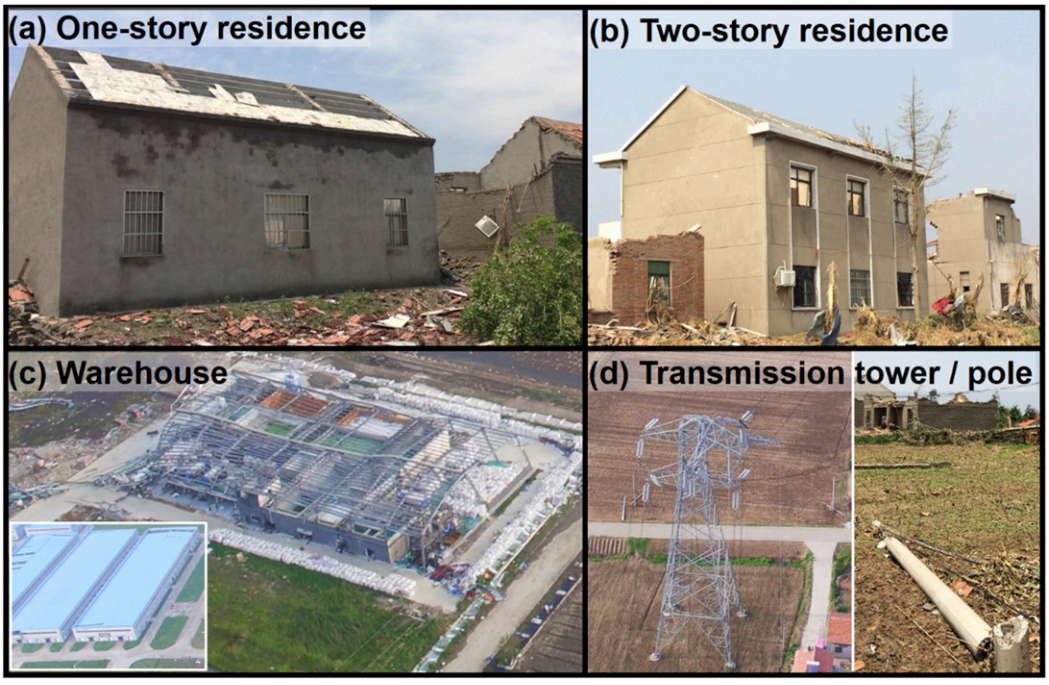

FIG. 13. Examples of damaged (a) one- and (b) two-story residences, (c) factory warehouses, and (d) transmission towers and poles within the tornado damage swath in Funing County, Yancheng, Jiangsu Province, China. The inset in (c) shows an example of nearby undamaged factory warehouses built using a metal building system.

The instances of damage along the tornado path were rated on the EF scale using the National Weather Service EF kit (LaDue and Mahoney 2006). The applicability of the EF scale, which is based on DIs in the United States, to several cities in China has been demonstrated in work by Meng and Yao (2014), Meng et al. (2016), and Bai et al. (2017). The primary DIs in this tornado case were one- and two-family residences, trees, transmission poles or towers, and some factory warehouses. The construction practices of one- and two-family residences in Yancheng are generally similar to those in the United States [refer to the examples described in WSEC (2006)]. Most of these residences are one story with gable roofs (Fig. 13a). The bearing walls of these residences mainly consist of unreinforced brick walls covered by a stucco veneer. There are also a few two- or three-story residences (Fig. 13b), which are usually constructed with reinforced concrete structural frames and unreinforced brick walls covered by a stucco veneer. Most of the factory warehouses are metal building systems with single-bay rigid frames, Z- or C-shaped purlins, and girts that span between rigid frames (Fig. 13c). This type of construction is comparable to some metal-building warehouses in the United States [refer to the examples of DI 21 in WSEC (2006)]. Transmission poles or towers (Fig. 13d), and trees [mainly aspens (hardwood) and pines (softwood)], were reasonably treated as the same as those in the United States.

Information from the aerial survey was primarily used to finalize EF-scale ratings due to the large extent of the damage area in this case. An aerial survey for such a high-impact deadly tornado event is crucial because it greatly aids a highly efficient survey process before the commencement of significant cleanup operations (e.g., Burgess et al. 2014). Furthermore, the aerial survey information is helpful for filling in the gaps in the ground damage surveys. The reliability of an EF rating based on an aerial survey has been demonstrated by Atkins et al. (2014) by comparing it with the EF rating based on an independent ground survey. In this study, the consistency between the aerial and ground survey–based EF ratings was checked at all the locations where ground surveys were also performed, and the results gave us confidence in rating the tornado intensity based on aerial surveys. Figure 14 shows an example of the reliability of using aerial survey videos (Fig. 14b) for a damage rating compared with a photo of the same damaged residence from the ground survey (Fig. 14a). The locations of the DIs from the aerial video were then marked on the high-resolution Google Earth satellite-view imagery that was taken on 12 May 2016 (e.g., Fig. 14c) to obtain whole-track EF isopleths. A post-tornado Google Earth image that was taken on 26 June 2016 was also shown for reference (Fig. 14d).

A complete tornado path and damage distribution were obtained based on both the ground and aerial damage surveys (Fig. 15). The damage swath was nearly straight, following an approximately west–east orientation, with a length of 34.5 km, a peak width of 4.1 km, and a life-span of about 50 min from around 1410 to 1500 LST. The analyzed tornado centerline was determined by tracking the continuous swath-scale convergent center of tree-fall patterns. Figure 16 shows one example of such a rotational center at Laowang village (its location is given in Fig. 15). The rotational tree-fall patterns were observed primarily near the tornado centerline (e.g., Fig. 16b; its aerial picture is given in Fig. 16c), while the convergent tree-fall patterns were observed both near or farther away from the tornado centerline (Figs. 16a,b). Such tree-fall patterns were also observed by Atkins et al. (2014) for the 2013 Moore, Oklahoma, EF5 tornado and the 2015 Foshan, Guangdong, tropical cyclone EF3 tornado (Bai et al. 2017). These tree-fall patterns were consistent with the simulated tree-fall patterns of strong tornadoes with tree-fall models (Karstens et al. 2013), in which trees fell before the arrival of the vortex centers, resulting in the appearance of tree fall with convergent flow removed from, and a rotational pattern close to, the vortex center.

The width of the damage swath was reasonably reliable based on a comparison between the wind estimations by the EF scale and the observed wind gusts near the DIs. During this event, there were two in situ surface weather stations that were located close to the damage swath of the Funing tornado. Station M5321, located about 200 m to the north of the EF0 isopleth between Jiqiao and Dalou villages (denoted in Fig. 15), recorded a maximum gust speed of 34.6 m s^{-1} at 1429 LST, which was the peak value that was observed during the whole event (Fig. 9d). This gust speed was within the EF0 range (29–38 m s^{-1}). About 615 m to the southeast of station M5321, an aspen [DI 27 in WSEC (2006)] was uprooted (Fig. 17). Another aspen located about 80 m farther southeast from the previous aspen was snapped. Because only 2 out of more than 20 aspens in this area were damaged, these two damaged trees were conservatively rated EF0 considering the uncertainties in EF ratings that are solely based on a small percentage of localized tree fall (e.g., Godfrey and Peterson 2017), which is not considered in WSEC (2006). Station M5325 was located at the edge of the EF0 isopleth near the beginning of the damage swath. The recorded gust speed had a peak of 22.5 m s^{-1} at 1416 LST, which was 6.5 m s^{-1} less than the lower limit in the EF0 range (29–38 m s^{-1}). This wind speed deviation probably resulted from the smoothing of the EF0 isopleth because

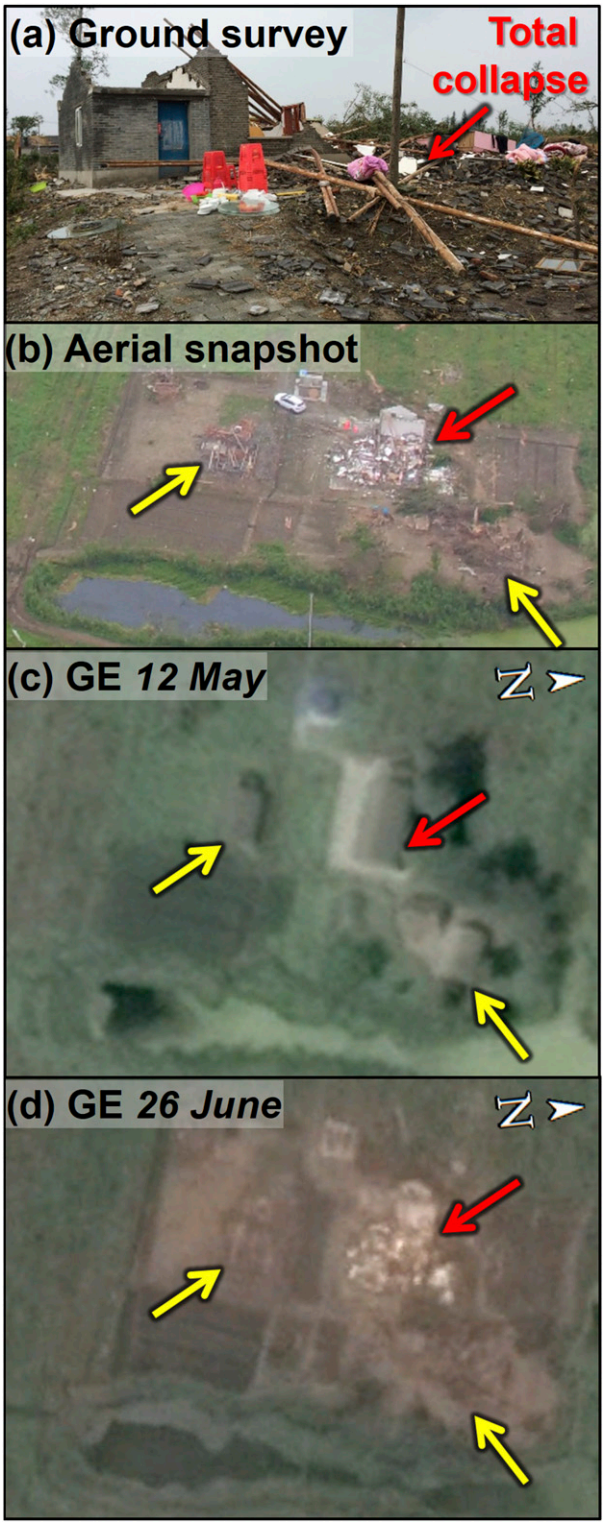

FIG. 14. Comparison of a damaged residence viewed from (a) the ground and (b) the drone. The Google Earth (GE) satellite-view imagery of this location taken on (c) 12 May and (d) 26 Jun 2016 are also shown for reference. The yellow arrows in (b)–(d) are plotted for location reference, and the red arrows in (a)–(d) indicate the same collapsed residence location.

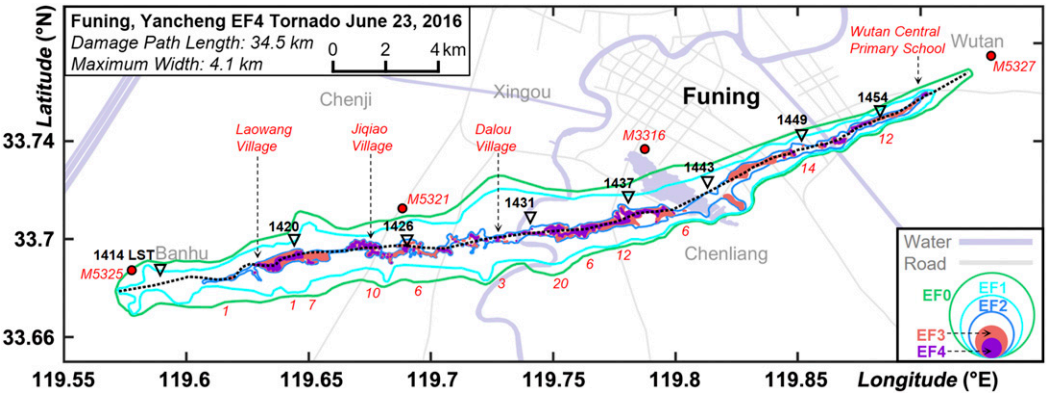

FIG. 15. Analyzed centerline (black dotted line) and EF isopleths of the 23 Jun 2016 Funing EF4 tornado. The triangles denote the locations of the 0.5° TVS at different times (LST). The black dashed arrows denote the rough locations of Laowang, Jiqiao, and Dalou villages, and the Wutan central primary school for reference. The red numbers near the southern edge of the damage swath denote the number of fatalities around the tornado center to the due north of the number location. The red dots represent in situ surface weather stations that were the nearest to the tornado damage swath during this event.

of sparsely damaged structures around this station. It could be reasonably assumed that the most severe ground damage close to the station was produced at the time when the station-observed gust speed reached its peak value during this event. Taking the smoothing in plotting the EF0 isopleth into account, these two comparisons supported the reliability of the EF0 isopleth determined in this study.

The strongest TVS was observed at the same time (around 1437 LST) and location as the most severe ground damage, which was at Chenliang Town (location given in Fig. 15). Station M3316, which was located about 1.1 km to the north of the EF0 isopleth in Chenliang (Fig. 15), recorded a peak gust of 19.2 m s^{-1} at 1437 LST (Fig. 9e). The damage swath was mainly located near the southern edge of the hook echo covering the 0.5° radial velocity pixels, with a magnitude greater than 22 m s^{-1} (Fig. 18). The 0.5° TVSs (denoted by inverted triangles in Fig. 15) during the whole tornado life-span were generally close to the tornado centerline.

The width (defined as the cross-track coverage of the EF0 isopleth) of the damage swath was generally larger during the first half of the tornado path, reaching a maximum value of 4.1 km in Dalou village and then, apparently, narrowed until the end (Fig. 15). Wide areas of straight-line winds were observed on both sides of the tornado centerline blowing toward the tornado center (e.g., Fig. 16a, in which each yellow arrow represents a clump of trees that fell in almost the same direction). The narrowing of the damage swath from 1437 LST (Fig. 15) was consistent with the weakening of the tornado vortex (in terms of TVSs) and contraction of the mesocyclone during its occlusion process.

The regions covered by isopleths of different EF levels had an apparently nonlinear variation (Fig. 15). The region covered by the EF1 isopleth was slightly smaller than that covered by the EF0 isopleth. The EF2 isopleth surrounded an area that was much narrower than the EF1 area, but it still extended almost the entire length of the tornado track. The difference in the EF1 and EF2 widths in the first half of the tornado path (from 1410 to about 1437 LST) was larger than in the second half. The EF3 isopleths were in close proximity to the EF2 isopleths along the entire tornado path, indicating a sharp increase in wind speeds in a narrow zone surrounding the tornado centerline. The EF3 damage was spotty, scattered from the beginning to near the end of the tornado centerline. Most of the EF3 damage accompanied the EF4 damage, even at the dissipating stage of the tornado, which could be why the fatalities (indicated by the red numbers along the damage swath in Fig. 15) were distributed along the whole tornado path.

Examples of damage rated EF4 are shown in Fig. 19a, showing completely collapsed residences, which were one-story buildings constructed of unreinforced brick walls with gable roofs. In addition to the collapsed residences, many other instances of severe damage were also observed around the tornado centerline. For example, several cars were thrown from the road (e.g., Fig. 19b) and an empty container (~2 t, 2 m wide, and 6 m long) was tossed about half a kilometer from its original site (Zheng et al. 2016; their Fig. 8e). Some trees were debarked (e.g., Fig. 19c). Numerous trees were uprooted (e.g., Fig. 19d), snapped, or twisted (e.g., Fig. 19e).

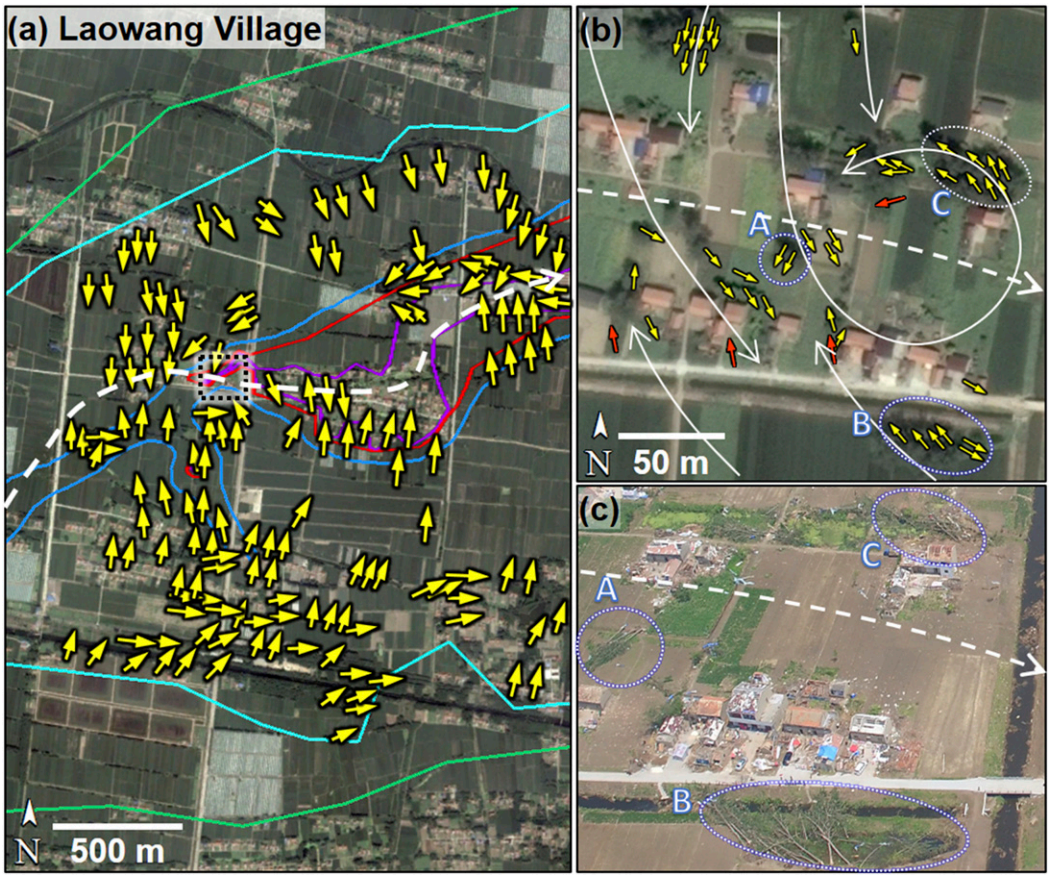

FIG. 16. (a) The tree fall (yellow arrows) at Laowang village (its location is given in Fig. 15) based on aerial videos and marked on the GE satellite-view imagery across the whole width of the damage swath. Each arrow represents a clump of trees that fell in almost the same direction. The EF0 (green), EF1 (cyan), EF2 (blue), EF3 (red), and EF4 (purple) isopleths are also shown. The area near the tornado centerline in the dashed box in (a) is enlarged in (b) with more detailed fallen directions of trees (yellow arrows) and transmission poles (short red arrows outlined in black) that were recorded in the ground survey. White solid curved arrows in (b) represent the general fallen directions of snapped transmission poles and fallen trees. (c) The aerial photo of the location in (b) taken by the drone during the survey is given, with A, B, and C denoting the same damaged trees in both panels. The analyzed tornado centerline is denoted by the white dashed curved arrow in all panels.

6. Discussion

This event provided the opportunity to review the efficacy of the integrated warning system for tornadoes in China, including the detection of tornadic storms using radar and other sensors, tornado nowcast and warning services, and public response.

There is considerable room for improvement in the SWATCH system. SWATCH inferred a tornado about 16 min after the start time of the Funing tornado, which indicates that the criteria used by SWATCH to infer a tornado may be too high. An improvement of the mesocyclone detection algorithm used for PUP, based on the climatological tornadic mesocyclone characteristics in China, may gain lead time and even reduce the false alarm ratio. Furthermore, the current version of SWATCH only displays mesonet wind observations that exceed a certain threshold within the past 30 min, rather than the highest spatial and temporal resolution data. In this way, the variability of surface wind patterns is not available. The mesonet stations are deployed with a spatial resolution of 4–30 km and a temporal resolution of 1 min, which could have been very helpful in monitoring variations in the mesoscale meteorological phenomena. Higher-resolution wind data at stations around the detected mesocyclone could be an important tool for monitoring tornadoes.

In addition to more effective radar guidance, a much earlier warning could have been issued, more confidently and more efficiently, if a tornado report was received during an earlier stage of the tornado, and if the meteorologists had more experience with these extreme events. Meteorological observatories

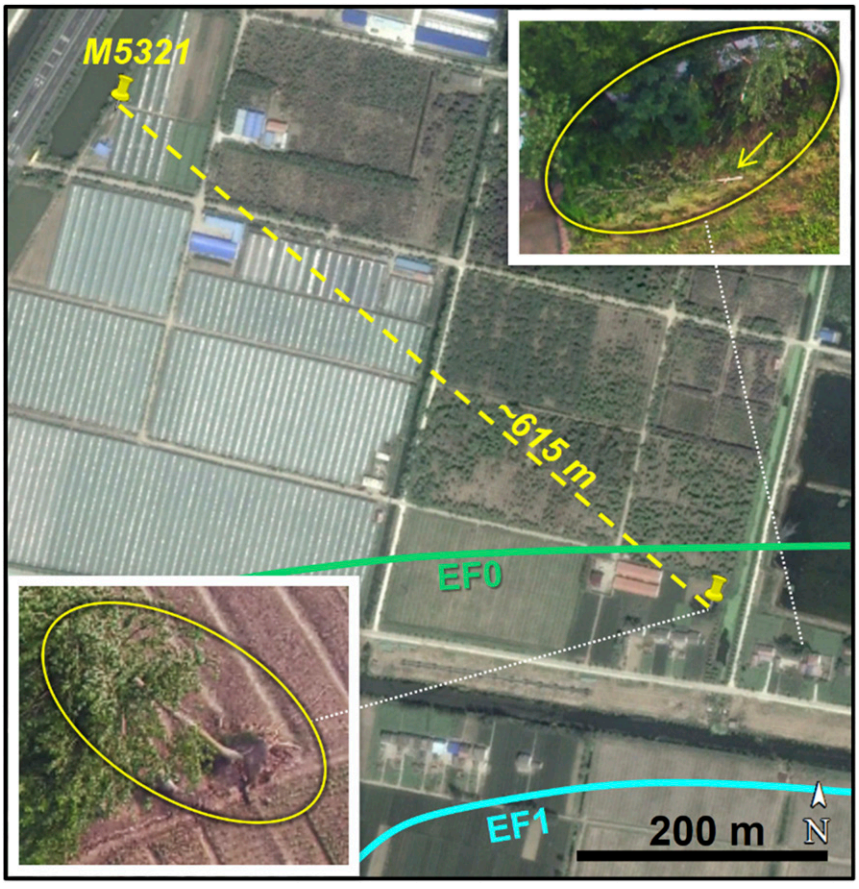

FIG. 17. The relative position between the in situ surface weather station M5321 and the nearest EF isopleths of the Funing tornado damage marked on the GE satellite-view imagery. Also shown are aerial photos of uprooted and snapped trees at two locations (denoted by dotted white lines) in the >EF0 area. The north direction and distance length scale are given in the bottom-right corner.

did not receive any tornado reports from local weather reporters[1] during the entire tornadic life cycle of this event. As a result, meteorological observatories were still issuing warnings of a potential tornado even though the tornado had already occurred. This points to the need for better training for local weather reporters. Forecasters also need advanced education and training for assessing tornado potential by integrating multiplatform observations. In particular, lower-level meteorological observatories may provide the possibility of gaining tornado warning lead time by concentrating on individual storm signatures.

The procedure for issuing tornado warnings needs to be made more efficient. After SWATCH inferred a tornado at 1426 LST, it took about 13 min for the Funing County–level meteorological observatory to issue a thunderstorm warning that mentioned the possibility of a tornado (1439 LST); this resulted in an even more negative lead time. In more detail, there was a 4-min time lag between SWATCH inferring a tornado and province-level forecasters making a nowcast containing a potential tornado, and there was another 9-min time lag between making a province-level nowcast containing a potential tornado and issuing a county-level thunderstorm warning that mentioned the potential for a tornado to the public.

[1] A local weather reporter is a local resident who agrees to report the occurrence of severe weather to a meteorological observatory—similar to a U.S. storm spotter, but with other duties in addition to spotting severe weather. They are usually directors of agriculture or hydrology stations or heads of a village or town. The duty of a local weather reporter includes 1) receiving and disseminating meteorological warnings; 2) collecting and reporting damage information; 3) popularizing meteorological science; 4) helping maintain local meteorological instruments; 5) observing and reporting local special weather phenomena; 6) helping with local meteorological disaster preparedness and mitigation; 7) helping with meteorological damage investigation and assessment; and 8) helping collect requirements, suggestions, and feedback on meteorological services.

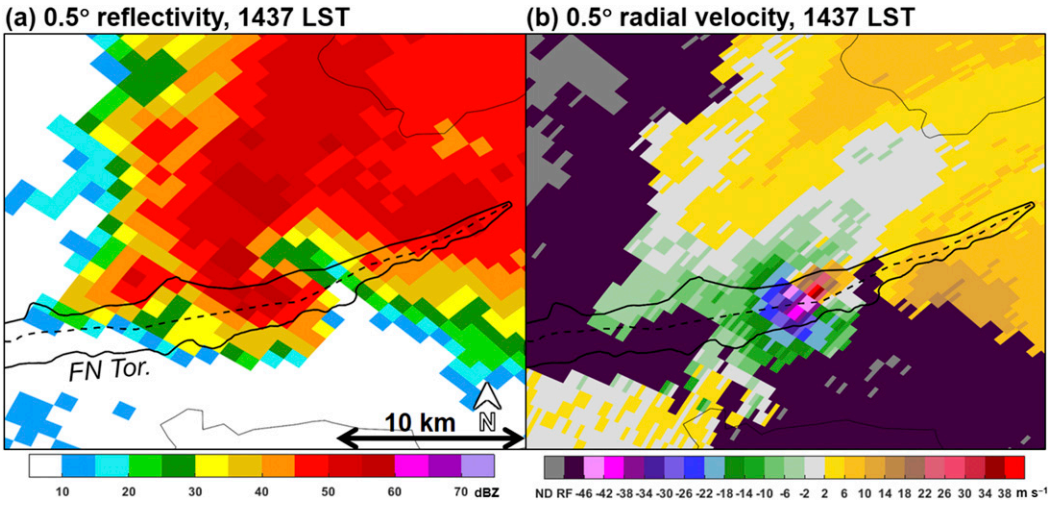

FIG. 18. (a) Base reflectivity (shaded; dBZ) and (b) radial velocity (shaded; m s^{-1}) at the 0.5° elevation angle from the Yancheng radar at 1437 LST 23 Jun 2016. The EF0 isopleth of the Funing tornado damage swath (thick black contour) and the analyzed tornado centerline (dashed) are also shown. The north direction and distance length scale are given at the bottom in (a).

In the Funing tornado event, even though the tornado warning was issued ~30 min before the demise of the Funing tornado, there were still many fatalities toward the end of the tornado path (Fig. 15). This could be a result of the limited efficiency in disseminating the warning and/or point toward the need for improvements

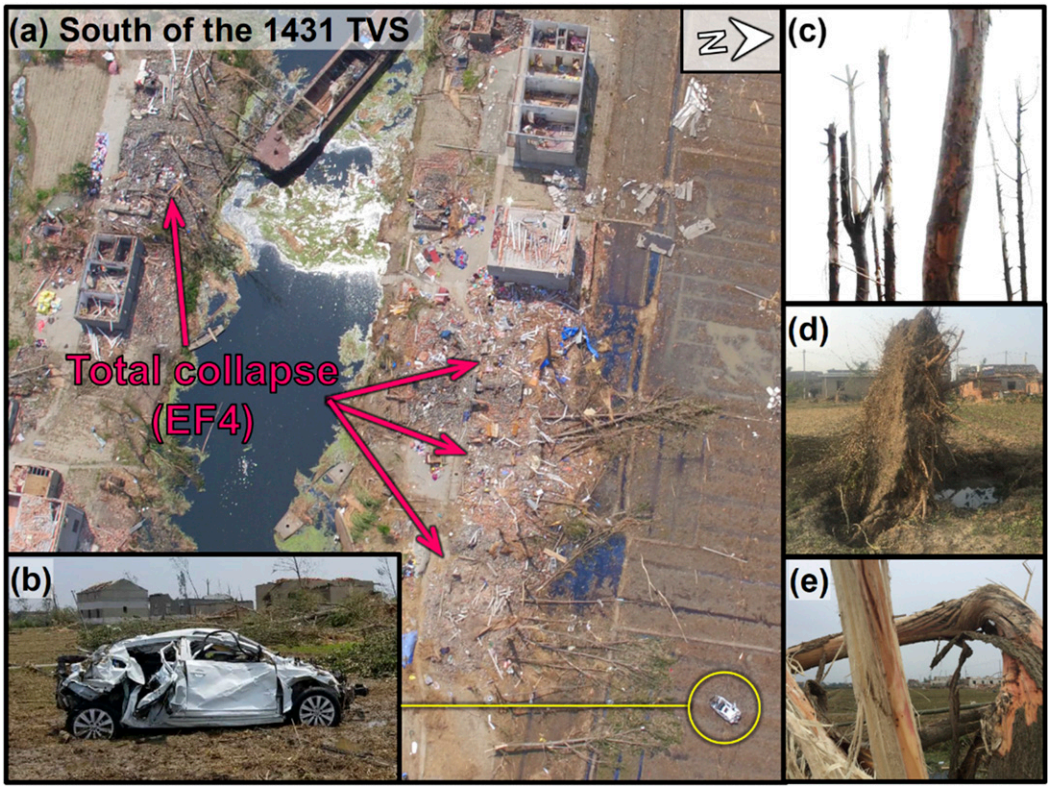

FIG. 19. (a) Instances of damaged residences rated EF4 on the south side of the tornado centerline near the TVS at 1431 LST, as shown in Fig. 15, with (b) a thrown car enlarged. The north direction is given in the top-right corner. Instances of (c) debarked, (d) uprooted, and (e) twisted trees caused by the Funing tornado are also shown.

in the public response to warnings (e.g., Doswell et al. 1999). Although the tornado occurrence in Jiangsu Province is climatologically the highest in China, the public in Jiangsu Province may still be unprepared for tornado events. In the ground survey, many local aging residents told the authors that they had only heard of tornadoes but never seen a tornado and did not know a tornado could cause such severe destruction. There is an urgent need to popularize the basic tornado knowledge and implement community response education to a tornado warning and related warning policy and policy changes. Well-educated local weather reporters serving as ambassadors between the meteorological observatories and the public may speed up this process.

7. Summary

This paper presents the storm environment, radar signatures, and damage distribution of the EF4 tornado event that occurred in Funing County, Yancheng, Jiangsu Province, China, during ~1410–1500 LST 23 June 2016. Causing 98 fatalities and 846 injuries, the Funing tornado became the deadliest tornado in China in the past 40 years and left a damage swath 34.5 km long with a maximum width of 4.1 km. The convective environment was quite favorable for the formation of a tornadic storm, with a 0–6-km bulk wind difference of 27.2 m s^{-1}, a strong clockwise-turning low-level directional shear, and a very moist layer within 1 km AGL. The 0–1-km storm-relative helicity was between the 50th and 75th percentiles of the U.S. climatology of the tornadic supercell environment. The tornadic mesocyclone had a maximum measurable altitude of 8 km AGL and a maximum rotational velocity of 42.2 m s^{-1} at the 0.5° elevation angle. The peak 0.5° rotational velocity within a cyclonic azimuthal shear radar signature (with a diameter no greater than 10 km) was close to the median of that associated with EF4+ tornadoes in the U.S. climatology (Smith et al. 2015). About 12 min after the appearance of the maximum rotational velocity of the mesocyclone, the TVS realized its maximum gate-to-gate azimuthal radial velocity difference of 84.5 m s^{-1} at the 0.5° elevation angle, corresponding to the most severe ground damage. The Funing tornado dissipated shortly after the occlusion process of the original mesocyclone. The new mesocyclone spawned a tornado in Sheyang County about 10 min after the demise of the Funing tornado.

Using the real-time rapidly updating SWATCH platform, meteorological observatories were quite successful in forecasting and issuing warnings for the severe weather hazards, but understated the tornado risk. The possibility of a tornado was first mentioned in a warning that was issued in the middle of the tornado's life-span. The tornado warning could have been issued earlier if 1) the per minute surface observations were made available in the SWATCH platform and 2) the tornado was reported to the local meteorological observatory in a timely manner. The forecasting and warning experience of Jiangsu Meteorological Bureau in this tornado case suggests that more lives could have been saved by more efficient monitoring, reporting, warning, and response strategies.

Although tornadoes are a somewhat rare weather phenomenon in China, they are nonetheless a significant threat to human life and property when they occur, especially given the level of economic development and the recent increase in population in tornado-prone areas, such as Jiangsu and Guangdong Provinces in China. This Funing tornado event, together with several high-impact tornado events in China in recent years, has motivated CMA to take action on regulating tornado reporting and testing quasi-operational tornado monitoring and warning systems. Starting in spring 2017, CMA has been developing an improved tornado reporting system and has been performing quasi-operational tests of tornado monitoring and warning in five provinces (Jiangsu, Anhui, Hubei, Zhejiang, and Guangdong) that have high tornado occurrence frequency.

In addition to the above efforts being made in the operational community, an increasing amount of research into tornadoes in China is being conducted, including a key national project known as "Observation, Prediction and Analysis of Severe Convection of China (OPACC)" (Xue 2016)—which was supported by the Ministry of Science and Technology of China from 2013 to 2017. One aspect of the project was tornado research. Another five-year key project "The Formation Mechanism and Predictability of Tornadoes in China"—which is supported by National Natural Science Foundation of China—was started in January 2018. These research efforts will provide scientific reference and guidance for current tornado monitoring and warning testing. In the future, more research efforts are needed to obtain a better understanding of tornadoes in China, to influence decision-makers in developing tornado preparedness and response programs, to drive meteorological agencies to improve the monitoring and recording of tornado occurrence, to stimulate the scientific community to better understand the local environment of tornadogenesis, and eventually to lead to the development of an operational tornado forecasting and warning system.

Acknowledgments. We thank the Funing Meteorological Bureau for support. We also thank the editor and three anonymous reviewers for their valuable and

constructive suggestions. This work was supported by the National Natural Science Foundation of China (41425018 and 41375048), the Ministry of Science and Technology of China (2013CB430104), and the National Natural Science Foundation of China (41461164006).

REFERENCES

Antonescu, B., D. M. Schultz, A. Holzer, and P. Groenemeijer, 2017: Tornadoes in Europe: An underestimated threat. *Bull. Amer. Meteor. Soc.*, **98**, 713–728, https://doi.org/10.1175/BAMS-D-16-0171.1.

Atkins, N. T., K. M. Butler, K. R. Flynn, and R. M. Wakimoto, 2014: An integrated damage, visual, and radar analysis of the 2013 Moore, Oklahoma, EF5 tornado. *Bull. Amer. Meteor. Soc.*, **95**, 1549–1561, https://doi.org/10.1175/BAMS-D-14-00033.1.

Bai, L., and Coauthors, 2017: An integrated damage, visual, and radar analysis of the 2015 Foshan, Guangdong, EF3 tornado in China produced by the landfalling Typhoon Mujigae (2015). *Bull. Amer. Meteor. Soc.*, **98**, 2619–2640, https://doi.org/10.1175/BAMS-D-16-0015.1.

Burgess, D. W., and Coauthors, 2014: 20 May 2013 Moore, Oklahoma, tornado: Damage survey and analysis. *Wea. Forecasting*, **29**, 1229–1237, https://doi.org/10.1175/WAF-D-14-00039.1.

Doswell, C. A., III, A. R. Moller, and H. E. Brooks, 1999: Storm spotting and public awareness since the first tornado forecasts of 1948. *Wea. Forecasting*, **14**, 544–557, https://doi.org/10.1175/1520-0434(1999)014<0544:SSAPAS>2.0.CO;2.

Dowell, D. C., and H. B. Bluestein, 2002a: The 8 June 1995 McLean, Texas, storm. Part I: Observations of cyclic tornadogenesis. *Mon. Wea. Rev.*, **130**, 2626–2648, https://doi.org/10.1175/1520-0493(2002)130<2626:TJMTSP>2.0.CO;2.

——, and ——, 2002b: The 8 June 1995 McLean, Texas, storm. Part II: Cyclic tornado formation, maintenance, and dissipation. *Mon. Wea. Rev.*, **130**, 2649–2670, https://doi.org/10.1175/1520-0493(2002)130<2649:TJMTSP>2.0.CO;2.

Fan, W., and X. Yu, 2015: Characteristics of spatial-temporal distribution of tornadoes in China (in Chinese with English abstract). *Meteor. Mon.*, **41**, 793–805.

French, M. M., and H. B. Bluestein, I. PopStefanija, C. A. Baldi, and R. T. Bluth, 2013: Reexamining the vertical development of tornadic vortex signatures in supercells. *Mon. Wea. Rev.*, **141**, 4576–4601, https://doi.org/10.1175/MWR-D-12-00315.1.

Godfrey, C. M., and C. J. Peterson, 2017: Estimating enhanced Fujita scale levels based on forest damage severity. *Wea. Forecasting*, **32**, 243–252, https://doi.org/10.1175/WAF-D-16-0104.1.

He, Z., Q. Zhang, L. Bai, and Z. Meng, 2017: Characteristics of mesoscale convective systems in central East China and their reliance on atmospheric circulation patterns. *Int. J. Climatol.*, **37**, 3276–3290, https://doi.org/10.1002/joc.4917.

Karstens, C. D., W. A. Gallus, B. D. Lee, and C. A. Finley, 2013: Analysis of tornado-induced tree fall using aerial photography from the Joplin, Missouri, and Tuscaloosa–Birmingham, Alabama, tornadoes of 2011. *J. Appl. Meteor. Climatol.*, **52**, 1049–1068, https://doi.org/10.1175/JAMC-D-12-0206.1.

LaDue, J. G., and E. A. Mahoney, 2006: Implementing the new enhanced Fujita scale within the NWS. *23rd Conf. on Severe Local Storms*, St. Louis, MO, Amer. Meteor. Soc., 5.5, https://ams.confex.com/ams/23SLS/techprogram/paper_115420.htm.

Markowski, P., and Y. Richardson, 2010: *Mesoscale Meteorology in Midlatitudes*. Wiley-Blackwell, 407 pp.

Meng, Z., and D. Yao, 2014: Damage survey, radar, and environment analyses on the first-ever documented tornado in Beijing during the heavy rainfall event of 21 July 2012. *Wea. Forecasting*, **29**, 702–724, https://doi.org/10.1175/WAF-D-13-00052.1.

——, D. Yan, and Y. Zhang, 2013: General features of squall lines in East China. *Mon. Wea. Rev.*, **141**, 1629–1647, https://doi.org/10.1175/MWR-D-12-00208.1.

——, and Coauthors, 2016: Wind estimation around the shipwreck of Oriental Star based on field damage surveys and radar observations. *Sci. Bull. (Beijing)*, **61**, 330–337, https://doi.org/10.1007/s11434-016-1005-2.

Rasmussen, E. N., 2003: Refined supercell and tornado forecast parameters. *Wea. Forecasting*, **18**, 530–535, https://doi.org/10.1175/1520-0434(2003)18<530:RSATFP>2.0.CO;2.

——, and D. O. Blanchard, 1998: A baseline climatology of sounding derived supercell and tornado forecast parameters. *Wea. Forecasting*, **13**, 1148–1164, https://doi.org/10.1175/1520-0434(1998)013<1148:ABCOSD>2.0.CO;2.

Richter, H., K. Turner, B. Guarente, and A. Smith, 2017: Radar signatures for severe convective weather: Mid-level mesocyclone. MetEd, COMET Program, UCAR, http://www.meted.ucar.edu/radar/severe_signatures/print_midlevel_mesocyclone.htm.

Smith, B., R. Thompson, A. Dean, and P. Marsh, 2015: Diagnosing the conditional probability of tornado damage rating using environmental and radar attributes. *Wea. Forecasting*, **30**, 914–932, https://doi.org/10.1175/WAF-D-14-00122.1.

Stumpf, G. J., A. Witt, E. D. Mitchell, P. L. Spencer, J. T. Johnson, M. D. Eilts, K. W. Thomas, and D. W. Burgess, 1998: The National Severe Storms Laboratory Mesocyclone Detection Algorithm for the WSR-88D. *Wea. Forecasting*, **13**, 304–326, https://doi.org/10.1175/1520-0434(1998)013<0304:TNSSLM>2.0.CO;2.

WDTD, 2017: The Radar and Applications Course convective storms structure and evolution. NOAA/NWS/Warning Decision Training Division, http://training.weather.gov/wdtd/courses/rac/outline.php.

WSEC, 2006: A recommendation for an enhanced Fujita scale (EF-scale). Wind Science and Engineering Center Rep., Texas Tech University, 111 pp., www.depts.ttu.edu/nwi/Pubs/FScale/EFScale.pdf.

Xie, Z., and C. Bueh, 2015: Different types of cold vortex circulations over northeast China and their weather impacts. *Mon. Wea. Rev.*, **143**, 845–863, https://doi.org/10.1175/MWR-D-14-00192.1.

Xue, M., 2016: Preface to the special issue on the "Observation, Prediction and Analysis of severe Convection of China" (OPACC) National "973" project. *Adv. Atmos. Sci.*, **33**, 1099–1101, https://doi.org/10.1007/s00376-016-0002-3.

——, K. Zhao, M. J. Wang, Z. H. Li, and Y. G. Zheng, 2016: Recent significant tornadoes in China. *Adv. Atmos. Sci.*, **33**, 1209–1217, https://doi.org/10.1007/s00376-016-6005-2.

Zheng, Y., and Coauthors, 2016: Wind speed scales and rating of the intensity of the 23 June 2016 tornado in Funing County, Jiangsu Province (in Chinese with English abstract). *Meteor. Mon.*, **42**, 1289–1303.

Zhu, X., and J. Zhu, 2004: New generation weather radar network in China (in Chinese with English abstract). *Mater. Sci. Technol.*, **32**, 255–258.